Gold Nanoparticle Decoration of Insulating Boron Nitride Nanosheet on Inert Gold Electrode Towards an Efficient Electrocatalyst for the Reduction of Oxygen to Water

Ganesan Elumalai,[a,b] Hidenori Noguchi,[a,b,c] Andrey Lyalin,[a] Tetsuya Taketsugu,[a,b,d] and Kohei Uosaki[a,b,c *]

[a]*Global Research Center for Environment and Energy based on Nanomaterials Science (GREEN), National Institute for Materials Science (NIMS), Tsukuba 305-0044, Japan*

[b]*Graduate School of Chemical Sciences and Engineering, Hokkaido University, Sapporo 060-0810, Japan*

[c]*International Center for Materials Nanoarchitectonics (WPI-MANA), National Institute for Materials Science (NIMS), 1-1 Namiki, Tsukuba 305-0044, Japan*

[d]*Department of Chemistry, Faculty of Science, Hokkaido University, Sapporo 060-0810, Japan*

Corresponding Authors

Tel: +81 29 860 4301; fax: +81 29 851 3362

E-mail address: UOSAKI.Kohei@nims.go.jp (Kohei Uosaki)

Abstract

Overpotential for oxygen reduction reaction (ORR) at Au electrode is reported to be reduced by 0.27 V by the modification with boron nitride nanosheet (BNNS) but oxygen is reduced only to H_2O_2 by 2-electron process as at Au electrode. Here we demonstrate that the decoration of BNNS with gold nanoparticles (AuNP) not only reduces the overpotential for ORR further by ca. 50 mV, but also opens a 4-electron reduction route to water. Both rotating disk electrode experiments with Koutecky-Levich analysis and rotating ring disk electrode measurements show that more than 50% of oxygen is reduced to water via 4-electron process at Au-BNNS/Au electrode while less than 20 and 10 % of oxygen are reduced to water at the BNNS/Au and bare Au electrodes, respectively. Theoretical analysis of free energy profiles for ORR at the BN monolayer with and without Au_8 cluster placed on Au(111) show significant stabilization of adsorbed oxygen atom by the Au_8 cluster, opening a 4-electron reduction pathway.

Key words: Fuel cell, Boron nitride, Oxygen reduction reaction, Gold nanoparticle, Gold electrode

1. Introduction

Large overpotential for oxygen reduction reaction (ORR) is one of the most crucial problems to be solved in the development of fuel cells [1-4] and there are worldwide efforts to develop novel electrocatalysts for ORR with high efficiency and long term stability based on low cost and abundant materials including non−precious metals and their alloys [1, 2, 5-11], metal oxides [12], metal nitrides [13, 14], metal oxynitrides [15, 16], metal carbides [14, 17], and N- and B-doped carbon materials with and without metal doping [18-22]. N- and B-doped carbon materials have been well studied as possible candidates of precious metal free efficient ORR catalysts. Recently, we theoretically predicted that hexagonal boron nitride (h-BN) placed on various metal substrates would act as an effective electrocatalyst for ORR [23-25] and experimentally proved [25, 26] that Au electrodes modified with various types of h-BN indeed act as effective ORR electrocatalysts. Overpotential for ORR at gold electrode is reduced by 0.27 V by the modification with BN nanosheet (BNNS), although it is still high compared with Pt electrode and oxygen is mainly reduced to H_2O_2 via 2-electron process [25, 26]. Substrate dependencies suggest that the interaction between BN and Au plays essential role for ORR activity [26]. Thus, one would expect higher ORR activity by increasing BN - Au interactions. There are several methods to increase the interaction and one of them is to deposit gold nanoparticles (AuNPs) on BNNS (Au-BNNS), which is then placed on a Au electrode (Au-BNNS/Au). In this communication, we have investigated the electrocatalytic properties of Au-BNNS/Au for ORR and found that not only the overpotential is reduced further by ca. 50 mV but also 4-electron reduction path way to water is opened by the decoration of BNNS with gold nanoparticles. Theoretical analysis suggests that increased stabilization of adsorbed oxygen atom by Au nanocluster leads to the 4-electron reduction.

2. Experimental

2.1 Materials

Ultrapure reagent grade H_2SO_4, isopropyl alcohol (IPA), $HAuCl_4$ (99.9%), $NaBH_4$, ethanol and acetone were purchased from Wako Pure Chemicals. Water was purified using Milli-Q system (Yamato, WQ-500). BN powder (99%) was purchased from High Purity Chemicals (BBIO3PB4).

2.2 Preparation of Au electrode modified with AuNP decorated BNNS (Au-BNNS/Au)

BNNS were prepared by a modified Hummer's method [27]. BN powder was thermally treated at 1050 ºC in Ar atmosphere in a tubular furnace for 1 hr to exfoliate the BN powder into BNNS. Then, 20 mg of BNNS was dispersed in 60 ml IPA solution and sonicated about 3 hr. 4 ml of 10 mM $HAuCl_4$ aqueous solution was added slowly to the N_2 saturated BNNS dispersed IPA solution under N_2 atmosphere and stirred well about 30 min. To decorate BNNS with AuNPs, 2 ml of 50 mM $NaBH_4$ aqueous solution was added drop wise to the above reaction mixture and stirred well for 4 hr [28, 29]. The products was collected by filtering (Whatman, pore size: 0.1 µm) and washed with ultra-pure water and ethanol. The obtained pink colour product was dried at 100 °C in vacuo for overnight. 15 µl of the dispersion of 1mg/3ml of BNNS or Au-BNNS in IPA solvent was spin coated on the Au electrode at 500 rpm and then the modified electrodes were dried at 100 °C for 30 min in vacuo.

2.3 XRD, TEM and Electrochemical measurements

X-ray diffraction (XRD) and transmission electron microscope (TEM) measurements were carried out using Altimat-2200 (Rigaku) with monochromatic Cu-Kα radiation (λ=1:5406 Å) and JEM-2100F (JEOL), respectively. Electrochemical measurements were carried out in three electrode configuration. Pt wire and Ag/AgCl (sat'd NaCl)

electrodes were used as a counter and a reference electrode, respectively. A dual potentiostat/function generator (Hokuto Denko, HR101B/HB111) and a rotation control unit (Pine Research, AFMSRCE02) were used to control the potential and the rotation rate of rotating (ring) disk electrode, respectively. All the electrochemical measurements were carried out in Ar or O_2 saturated 0.5 M H_2SO_4 solution at room temperature. All electrodes were pre-treated by cycling the potential between -0.1 and +1.5 V at a sweep rate of 100 mV/s for 100 cycles.

3. Results and discussion

Figure 1(A) shows XRD patterns of the (i) BNNS and (ii) Au-BNNS. While only the diffraction peaks corresponding to pure h-BN were observed for BNNS, peaks corresponding to Au were observed for Au-BNNS [30, 31]. The average crystallite size of Au particles was estimated to be ca. 30 nm using Debye-Scherrer equation [32]. Figure 1(B) shows low ((a), (c)) and high ((b), (d)) resolution TEM images of BNNS ((a), (b)) and Au-BNNS ((c), (d)). HRTEM image of BNNS with FFT (Figure 1(B)(b)) shows BNNS are composed of a single to few layers of h-BN as already reported [25]. AuNPs are randomly distributed on BNNS surface as shown in Figure 1(B)(c). Figure 1(B)(d) shows the lattice images of AuNPs with and the size of AuNPs on BNNS ranges between 5 to 30 nm, which is in good agreement with XRD results.

Figure 2(A) shows linear sweep voltammograms (LSVs) of (a) bare Au, (b) BNNS/Au, (c) Au-BNNS/Au, and (d) bare Pt disk electrodes in RDE configuration with various rotation rates with a potential scan of negative direction of 10 mV/s measured in 0.5 M H_2SO_4 solution. The potentials at which ORR current becomes -0.02 mA/cm^2 are 210, 480, 530 and 770 mV at the bare Au, BNNS/Au, Au-BNNS/Au, and bare Pt electrodes [33], respectively. Overpotential for ORR at BNNs/Au electrode was reduced by 50 mV by the

AuNP decoration. Although it does not look significant, one must note that not only the current-voltage relation is shifted towards positive potential direction but also the limiting current at a given rotation rate became higher, suggesting that number of electrons involved in the ORR is larger at the Au-BNNS/Au electrode than at the BNNS/Au electrode.

This can be quantitatively analyzed by utilizing Koutecky-Levich (K-L) equations (Eq. (1)).

$$1/i = 1/i_k + 1/B\omega^{1/2} \qquad (1)$$

Here B is given by:

$$B = 0.620\mathrm{n}FC_{O2}^{*}D^{2/3}v^{-1/6} \qquad (2)$$

where n is the number of electrons transferred in the overall reaction process, F is the Faraday constant (96490 C mol^{-1}), v is the kinematic viscosity ($0.01 cm^2 s^{-1}$) [34], D and C_{O2} are the diffusion coefficient and the bulk concentration (1.1×10^{-6} mol cm^{-3}) of the oxygen [35, 36], ω is the rotation rate, and i_k is the kinetic current without any mass transfer limitation, which is given by:

$$i_k = \mathrm{n}FAkC_{O2}^{*} \qquad (3)$$

Thus, one expects a linear relation between $1/i$ and $1/\omega^{1/2}$ (K-L plot). The extrapolation of this relation to $1/\omega^{1/2} = 0$ yields $1/i_k$ and, then, the rate constant k can be obtained from Eq. (3).

K-L plots of each electrode at various potentials are shown as the inset of each figure. Linear relations are observed in all cases and the number of electrons transferred at each electrode potential is calculated to be ca. 2 for (a) the bare Au and (b) BNNS/Au electrodes, ca. 4 for (d) the bare Pt electrode, and ca. 3 for (c) the Au-BNNS/Au electrode, suggesting the partial generation of H_2O_2 and H_2O at the Au-BNNS/Au electrode.

Partial generation of H_2O_2 and H_2O can be directly probed by using RRDE, in which H_2O_2 generated at the disk electrode during ORR can be detected at the ring electrode. Bottom and top panels of Figure 2(B) show the disk current at the (i) bare Au, (ii) BNNS/Au, (iii) Au-BNNS/Au, and (iv) bare Pt disk electrodes, and corresponding currents at the Pt ring electrode, respectively, as a function of the disk potential obtained with the rotation rate of 1500 rpm. The ring potential was kept at 900 mV so that the ring current corresponds to the oxidation of H_2O_2 generated at the disk electrode [37].

As soon as cathodic current due to ORR started to flow at the (i) bare Au and (ii) BNNS/Au electrodes, ring current started to flow and increased with the disk current as potential was scanned to negative direction. Oxygen is known to be reduced to H_2O_2 via 2-electron process at Au electrode [38]. At the bare Pt disk electrode, while the disk current is about twice of that at the bare Au electrode in diffusion limited region, no significant ring current was observed, showing O_2 is reduced to H_2O via 4-electron process [4]. At the BNNS/Au electrode, disk current was larger and ring current was also larger accordingly than at the Au electrode, showing oxygen is mainly reduced to H_2O_2 via 2-electron process as at the bare Au electrode. At the Au-BNNS/Au electrode, however, although disk current was larger than at the bare Au electrode, ring current became about half of that at the bare Au electrode, suggesting the partial generation of H_2O_2 and H_2O.

Fraction of H_2O generation can be estimated quantitatively by using the number of electrons transferred during ORR determined by the K-L analysis (2 for H_2O_2 generation and 4 for H_2O generation) and also by analyzing the results of RRDE using Eqs. (4) and (5) [39]:

$$\chi_{H2O2} = [(2I_{ring} / N) / (I_{disk} + I_{ring} / N)] \times 100 \quad (4)$$

$$\chi_{H2O} = 100 - [(2I_{ring} / N) / (I_{disk} + I_{ring} / N)] \times 100 \quad (5)$$

where χ_{H2O2} and χ_{H2O} are the fractions of H_2O_2 and H_2O generation, respectively, I_{disk} and I_{ring} are the disk and ring currents, respectively, and N is the collection efficiency of the RRDE electrode, which is 0.20 in this experiment. Figure 2(C) shows the fraction of H_2O generation at various electrodes as a function of potential calculated from the K-L plots (symbols) and RRDE measurements (solid lines). Both results are agreed reasonably well. Fraction of H_2O generation was ca. 0 and ca. 100% at the bare Au and bare Pt electrodes, respectively, as reported before. At the BNNS/Au and Au-BNNS/Au electrodes, about 20% and more than 50%, respectively, of oxygen are reduced to H_2O, confirming the important role of AuNP on BNNS for ORR to H_2O via 4-electron process. By AuNP modification of Au electrode, ORR overpotential is reduced by 200 mV but oxygen is reduced to H_2O_2 by 2-electron process [40]. The partial reduction of oxygen to H_2O_2 and H_2O has been also reported at other substrates modified with AuNPs [41, 42] but the overpotential for ORR is less and the fraction for H_2O generation is higher at Au-BNNS/Au electrode than the results previously reported.

To understand why 4-electron reduction becomes possible at the Au-BNNS/Au electrode, we have performed theoretical analysis of a free energy profile for intermediates of ORR on the model system consisting of a small Au_8 cluster supported on the monolayer BN on Au(111). All calculations are based on DFT with the functional of Wu and Cohen [43] as implemented in the SIESTA code [44]. The Au(111) surface is represented by the four-layer slab containing 7 × 7 unit cells of Au covered by the 8 × 8 element of h-BN. Calculations details are described previously [23-25]. Figure 3 shows the calculated free energy profiles for ORR at the BN monolayer with and without modification by a Au_8 cluster on Au(111). While Au_8 cluster on BN/Au(111) mildly stabilizes O_2^*, OOH^* and OH^* intermediates by 0.5 – 0.7 eV, it drastically stabilizes O^* by 1.6 eV in comparison with the adsorption at BN/Au(111) surface. Such stabilization of O^* on Au_8-BN/Au(111) makes the dissociation of

OOH^*, which is a uphill process at BN/Au(111) surface, downhill, opening a 4-electron reduction pass way of oxygen to H_2O..

Adsorption of sulfate anion is known to inhibit ORR at various electrodes [33, 45, 46] and it is also true here. At all electrodes, current – potential relations in oxygen saturated sulfuric acid solution are always observed at more negative potential than in perchlorate acid solution by 60, 50, 80 and 70 mV at bare Au, BNNS/Au, Au-BNNS/Au and bare Pt electrodes, respectively, showing the inhibition of ORR by adsorbed sulfate ion. More detailed investigation is under way.

The durability was tested not extensively but for continuous 3h potential scanning. Within this time (ca. 77 cycles), the activity was reduced only slightly.

4. Conclusion

In summary, AuNP decoration of BNNS/Au electrode not only reduces overpotential by 50 mV but also increases the fraction of oxygen to H_2O via 4-electron process. The overpotential for ORR at the Au-BNNS/Au electrode is ca. 320 mV less than that at the bare Au electrode. The fraction of H_2O generation via 4-electron process determined from the slope of K-L plot and RRDE measurements is more than 50%, while those at the bare Au and BNNS/Au electrodes are almost 0% and 20%, respectively. Theoretical analysis of free energy profiles for ORR at the BN monolayer with and without Au_8 cluster modification placed on Au(111) show drastic stabilization of adsorbed oxygen atom by Au_8 cluster, opening a 4-electron reduction pathway because the dissociation of adsorbed OOH, which is a uphill process at the BN monolayer on Au(111), becomes downhill process.

ACKNOWLEDGMENT

The present work was partially supported by the Development of Environmental Technology using Nanotechnology and World Premier International Research Center (WPI) Initiative on Materials Nanoarchitectonics from the Ministry of Education, Culture, Sports, Science and Technology (MEXT), Japan and by Grant-aid for Scientific Research from the Japan Society for the Promotion of Science (15K05387). The computations were partly performed at the Institute for Molecular Science.

References

[1] F. Colmati, E. Antolini, E.R. Gonzalez, Effect of temperature on the mechanism of ethanol oxidation on carbon supported Pt, PtRu and Pt_3Sn electrocatalysts, J. Power Sources 157 (2006) 98-103.

[2] M. Winter, R.J. Brodd, What Are Batteries, Fuel Cells, and Supercapacitors? Chem. Rev. 104 (2004) 4245-4269.

[3] M.H. Shao, K. Sasaki, R.R. Adzic, Pd-Fe Nanoparticles as Electrocatalysts for Oxygen Reduction, J. Am. Chem. Soc. 128 (2006) 3526-3527.

[4] N.M. Markovic, T.J. Schmidt, V. Stamenkovic, P.N. Ross, Oxygen Reduction Reaction on Pt and Pt Bimetallic Surfaces: A Selective Review, Fuel Cells 1 (2001) 105-116.

[5] A. Kongkanand, S. Kuwabata, G. Girishkumar, P. Kamat, Single-Wall Carbon Nanotubes Supported Platinum Nanoparticles with Improved Electrocatalytic Activity for Oxygen Reduction Reaction, Langmuir 22 (2006) 2392-2396.

[6] J. Zhang, K. Sasaki, E. Sutter, R.R. Adzic, Stabilization of Platinum Oxygen-Reduction Electrocatalysts Using Gold Clusters, Science 315 (2007) 220-222.

[7] B. Lim, M. Jiang, P.H.C. Camargo, E.C. Cho, J. Tao, X. Lu, Y. Zhu, Y. Xia, Pd-Pt Bimetallic Nanodendrites with High Activity for Oxygen Reduction, Science 324 (2009) 1302-1305.

[8] J. Zhang, H. Yang, J. Fangand, S. Zou, Synthesis and Oxygen Reduction Activity of Shape-Controlled Pt_3Ni Nanopolyhedra, Nano Lett. 10 (2010) 638-644.

[9] W. Chen, J. Kim, S. Sun, S. Chen, Electrocatalytic Reduction of Oxygen by FePt Alloy Nanoparticles, J. Phys. Chem. C 112 (2008) 3891-3898.

[10] Y. Xu, H. Wang, R. Zhu, C. Liu, X. Wu, B. Zhang, Conversion of CuO Nanoplates into Porous Hybrid Cu_2O/Polypyrrole Nanoflakes through a Pyrrole-Induced Reductive Transformation Reaction, Chem. – Asian J. 8 (2013) 1120-1127.

[11] G. Wu, P. Zelenay, Nanostructured Nonprecious Metal Catalysts for Oxygen Reduction Reaction, Acc. Chem. Res. 46 (2013) 1878-1889.

[12] X. Yu, S. Ye, Recent advances in activity and durability enhancement of Pt/C catalytic cathode in PEMFC Part II: Degradation mechanism and durability enhancement of carbon supported platinum catalyst, J. Power Sources 172 (2007) 145-154.

[13] Y. Shao, J. Liu, Y. Wang, Y. Lin, Novel catalyst support materials for PEM fuel cells: current status and future prospects, J. Mater. Chem. 19 (2009) 46-59.

[14] Y.J. Wang, D.P. Wilkinson, J. Zhang, Noncarbon Support Materials for Polymer Electrolyte Membrane Fuel Cell Electrocatalysts, Chem. Rev. 111 (2011) 7625-7651.

[15] B. Cao, G.M. Veith, R.E. Diaz, J. Liu, E.A. Stach, R.R. Adzic, P.G. Khalifah, Cobalt Molybdenum Oxynitrides: Synthesis, Structural Characterization, and Catalytic Activity for the Oxygen Reduction Reaction, Angew. Chem. Int. Ed. 52 (2013) 10753-10757; Angew. Chem. 125 (2013) 10953–10957.

[16] Y. Maekawa, A. Ishihara, J.H. Kim, S. Mitsushima, K. Ota, Catalytic Activity of

Zirconium Oxynitride Prepared by Reactive Sputtering for ORR in Sulfuric Acid, Electrochem. Solid-State Lett. 11 (2008) B109-B112.

[17] G. Zhong, H. Wang, H. Yu, F. Peng, A Novel Carbon-Encapsulated CobaltTungsten Carbide as Electrocatalyst for Oxygen Reduction Reaction in Alkaline Media, Fuel Cells 13 (2013) 387-391.

[18] R. Liu, D. Wu, X. Feng, K. Müllen, Nitrogen-Doped Ordered Mesoporous Graphitic Arrays with High Electrocatalytic Activity for Oxygen Reduction, Angew. Chem. Int. Ed. 49 (2010) 2565-2569; Angew. Chem. 122 (2010) 2619–2623.

[19] Z. S. Wu, S. Yang, Y. Sun, K. Parvez, X. Feng, K. Müllen, 3D Nitrogen-Doped Graphene Aerogel Supported Fe_3O_4 Nanoparticles as Efficient Electrocatalysts for the Oxygen Reduction Reaction, J. Am. Chem. Soc. 134 (2012) 9082-9085.

[20] R.A. Sidik, A.B. Anderson, N.P. Subramanian, S.P. Kumaraguru, B.N. Popov, O_2 Reduction on Graphite and Nitrogen-Doped Graphite: Experiment and Theory, J. Phys. Chem. B, 110 (2006) 1787-1793.

[21] J. Ozaki, T. Anahara, N. Kimura, A. Oya, Simultaneous doping of boron and nitrogen into a carbon to enhance its oxygen reduction activity in proton exchange membrane fuel cells, Carbon, 44 (2006) 3358-3378.

[22] K. Gong, F. Du, Z. Xia, M. Durstock, L. Dai, Nitrogen-Doped Carbon Nanotube Arrays with High Electrocatalytic Activity for Oxygen Reduction, Science 323 (2009) 760-764.

[23] A. Lyalin, A. Nakayama, K. Uosaki, T. Taketsugu, Functionalization of Monolayer h-BN by a Metal Support for the Oxygen Reduction Reaction, J. Phys. Chem. C 117 (2013) 21359-21370.

[24] A. Lyalin, A. Nakayama, K. Uosaki, T. Taketsugu, Theoretical predictions for hexagonal BN based nanomaterials as electrocatalysts for the oxygen reduction

reaction, Phys. Chem. Chem. Phys. 15 (2013) 2809-2820.

[25] K. Uosaki, G. Elumalai, H. Noguchi, T. Masuda, A. Lyalin, A. Nakayama, T. Taketsugu, Boron Nitride Nanosheet on Gold as an Electrocatalyst for Oxygen Reduction Reaction: Theoretical Suggestion and Experimental Proof, J. Am. Chem. Soc. 136 (2014) 6542-6545.

[26] G. Elumalai, H. Noguchi, K. Uosaki, Electrocatalytic activity of various types of h-BN for the oxygen reduction reaction, Phys. Chem. Chem. Phys., 16 (2014) 13755-13761.

[27] K.S. Subrahmanyam, A.K. Manna, S.K. Pati, C.N.R. Rao, A study of graphene decorated with metal nanoparticles, Chem. Phys. Lett. 497 (2010) 70-75.

[28] Y. Lin, C.E. Bunker, K.A.S. Ferno, J.W. Connell, Aqueously Dispersed Silver Nanoparticle-Decorated Boron Nitride Nanosheets for Reusable, Thermal Oxidation-Resistant Surface Enhanced Raman Spectroscopy (SERS) Devices, ACS Appl. Mater Interfaces 4 (2012) 1110-1117.

[29] G.-H. Yang, A. Abulizi, J.-J. Zhu, Sonochemical fabrication of gold nanoparticles–boron nitride sheets nanocomposites for enzymeless hydrogen peroxide detection, Ultrasonics Sonochemistry 21 (2014) 1958-1963.

[30] C.Y. Zhi, Y. Bando, C.C. Tan, D. Golberg, Effective precursor for high yield synthesis of pure BN nanotubes, *Solid State Commun.* **2005**, *135*, 67-70.

[31] L.D. Zhu, T.S. Zhao, J.B. Xu, Z.X. Liang, Preparation and characterization of carbon-supported sub-monolayer palladium decorated gold nanoparticles for the electro-oxidation of ethanol in alkaline media, *J. Power Sources* **2009**, *187*, 80-84.

[32] A. Patterson, The Scherrer Formula for I-Ray Particle Size Determination, *Phys. Rev.* **1939**, *56*, 978-982.

[33] J.X. Wang, N.M Markovic, R.R. Adzic, Kinetic Analysis of Oxygen Reduction on Pt(111) in Acid Solutions: Intrinsic Kinetci Parameters and Anion Adsorption effects, J. Phys. Chem. B 108 (2004) 4127-4133.

[34] M. Kullapere, G. Jürmann, T.T. Tenno, J.J. Paprotny, F. Mirkhalaf, K. Tammeveski, Oxygen Electroreduction on chemically modified glassy carbon electrodes in alkaline solution, J. Electroanal. Chem. 599 (2007) 183-193.

[35] K.E. Gubbins, R.D.J. Walker, The Solubility and Diffusivity of Oxygen in Electrolytic Solutions, J. Electrochem. Soc. 112 (1965) 469-471.

[36] R.E. Davis, G.L. Horvath, C.W. Tobias, The solubility and diffusion coefficient of oxygen in potassium hydroxide solutions, Electrochim. Acta 12 (1967) 287-297.

[37] O. Antoine, R. Durand, RRDE study of oxygen reduction on Pt nanoparticles inside Nafion: H_2O_2 production in PEMFC cathode conditions, J. Appl. Electrochem. 30 (2000) 839-844.

[38] R.R. Adzic, J. Lipkowski, P.N. Ross, Electrocatalysis Wiley/VCH, New York, 1998 (Chapter 5).

[39] N.M. Markovic, H.A. Gasteiger, N. Philip, Oxygen Reduction on Platinum Low-Index Single-Crystal Surfaces in Alkaline Solution: Rotating Ring Disk Pt(hkl) Studies, J. Phys. Chem. 100 (1996) 6715-6721.

[40] M.S. El-Deab, T. Ohsaka, An extraordinary electrocatalytic reduction of oxygen on gold nanoparticles-electrodeposited gold electrodes, *Electrochem. Comm.* 4 (2002) 288-292.

[41] V.A. Sethuraman, J.W. Weidner, A.T. Haug, S. Motupally, L.V. Protsailo, Hydrogen Peroxide Formation Rates in a PEMFC Anode and Cathode Effect of Humidity and Temperature, J. Electrochem. Soc. 155 (2008) B50-B57.

[42] I. Yagi, T. Ishida, K. Uosaki, Electrocatalytic reduction of oxygen to water at Au

nanoclusters vacuum-evaporated on boron-doped diamond in acidic solution, Electrochem. Commun. 6 (2004) 773-779.

[43] Z. Wu, R.E. Cohen, More accurate generalized gradient approximation for solids, Phys. Rev. B 73 (2006) 235116.

[44] D. Sánchez-Portal, P. Ordejón, E. Artacho, J.M. Soler, Density-Functional Method for Very Large Systems with LCAO Basis Sets, Int. J. Quantum Chem. 65 (1997) 453−461.

[45] N. Ohta, K. Nomura, I. Yagi, Adsorption and Electroreduction of Oxygen on Gold in Acidic Media: In Situ Spectroscopic Identification of Adsorbed Molecular Oxygen and Hydrogen Superoxide, J. Phys. Chem. C 116 (2012) 14390-14400.

[46] S. Tong, H. Noguchi, T. Masuda, K. Uosaki, Direct proof of potential dependent oxygen adsorption on a gold electrode surface by electrochemical quartz crystal microbalance, Electrochemistry Communications 34 (2013) 33–36.

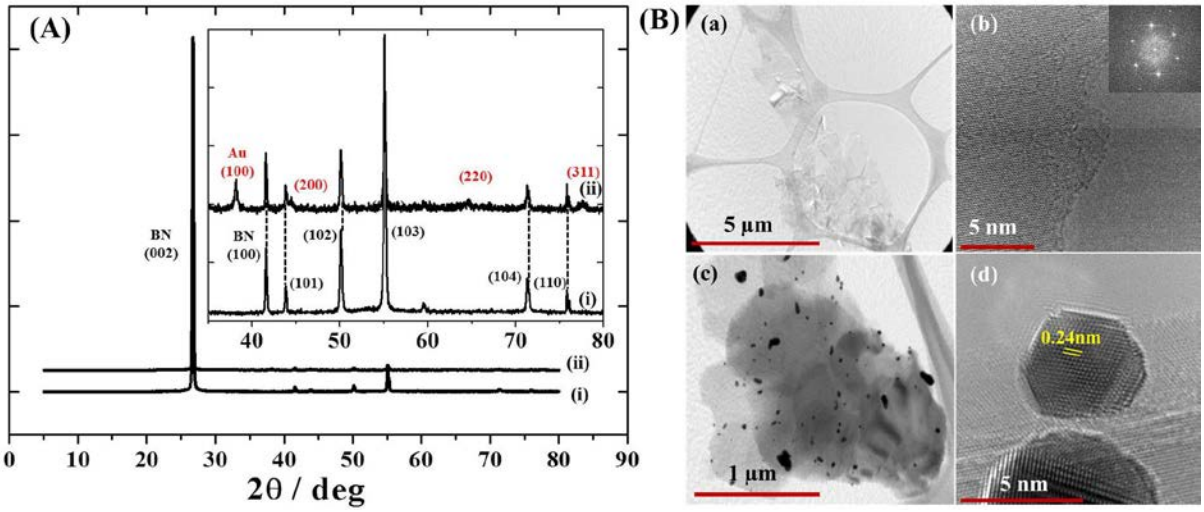

Figure1. (A) XRD patterns of (i) BNNS and (ii) Au-BNNS. Inset: Enlarged patterns. Diffraction peaks are marked by black and red for BN and Au peaks, respectively. (B) TEM images of BNNS ((a), (b)) and Au-BNNS ((c), (d)). Inset of (b) is the FFT of the central part of the image.

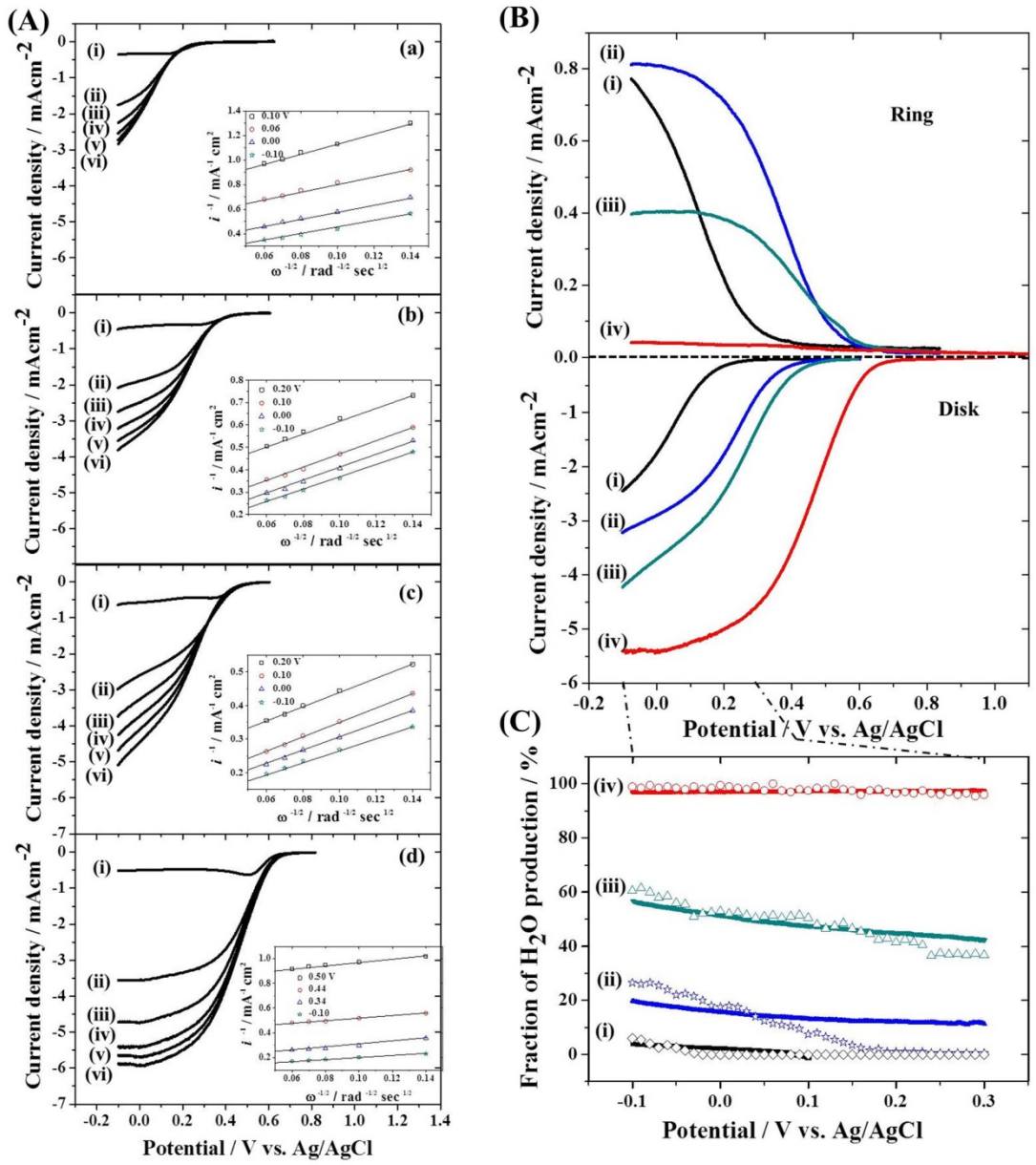

Figure 2. (A) LSVs of (a) bare Au, (b) BNNS/Au, (c) Au-BNNS/Au, and (d) Pt electrodes in O_2 saturated 0.5 M H_2SO_4 solution in RDE configuration with rotation rate of (i) 0, (ii) 500, (iii) 1000, (iv) 1500, (v) 2000, and (vi) 2500 rpm. Sweep rate: 10 mV/s. Insets: K-L plots of each electrode at various potentials. (B) Disk current at (i) bare Au, (ii) BNNS/Au, (iii) Au-BNNS/Au, and (iv) bare Pt electrodes (bottom panel) and corresponding ring current at a Pt ring electrode held at 900 mV (top panel) in RRDE configuration with the rotation rate of 1500 rpm as a function of disk potential measured in O_2 saturated 0.5 M H_2SO_4 solution with the sweep rate of 10mV/sec. (C) Fraction of H_2O generation as a function of potential at (i) bare Au, (ii) BNNS/Au, (iii) Au-BNNS/Au, and (iv) Pt electrodes determined from K-L plots (Figure 2(A)) (symbols) and RRDE (Figure 2(B)) measurements (solid lines).

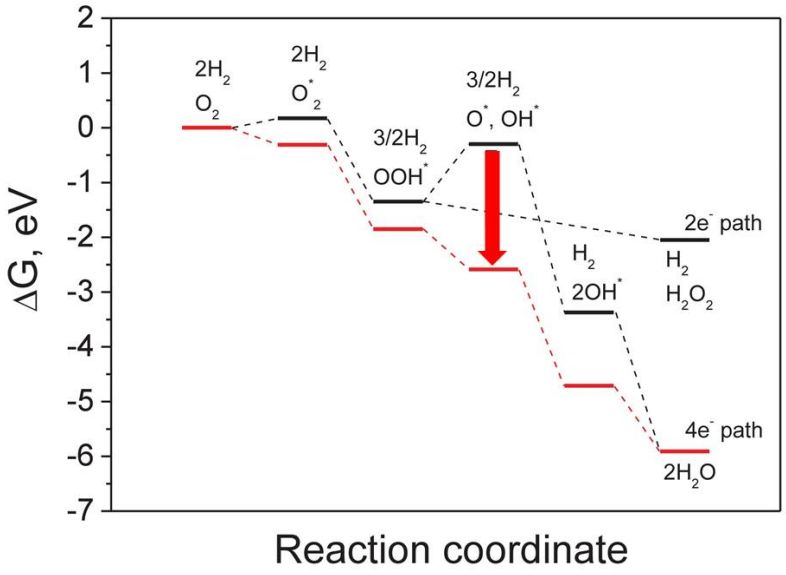

Figure: 3 Free energy diagrams for ORR at BN monolayer/Au(111) (black line) and Au_8-BN monolayer/Au(111) (red line) electrodes.